Atmos. Chem. Phys. Discuss., 11, 13355–13380, 2011
www.atmos-chem-phys-discuss.net/11/13355/2011/
doi:10.5194/acpd-11-13355-2011

Atmospheric Chemistry and Physics Discussions

Assimilating remotely sensed cloud optical thickness into a mesoscale model

D. Lauwaet[1,2], **K. De Ridder**[2], **and P. Pandey**[1,2]

[1]Physical and Regional Geography Research Group, Department of Earth and Environmental Sciences, K. U. Leuven, Celestijnenlaan 200 E, 3001 Heverlee, Belgium
[2]Vlaamse Instelling voor Technologisch Onderzoek (VITO), Boeretang 200, 2400 Mol, Belgium

Received: 13 April 2011 – Accepted: 19 April 2011 – Published: 2 May 2011

Correspondence to: D. Lauwaet (dirk.lauwaet@ees.kuleuven.be)

Published by Copernicus Publications on behalf of the European Geosciences Union.

Abstract

The Advanced Regional Prediction System, a mesoscale atmospheric model, is applied to simulate the month of June 2006 with a focus on the near surface air temperatures around Paris. To improve the simulated temperatures which show errors up to 10 K during a day on which a cold front passed Paris, a data assimilation procedure to calculate 3-D analysis fields of specific cloud liquid and ice water content is presented. The method is based on the assimilation of observed cloud optical thickness fields into the Advanced Regional Prediction System model and operates on 1-D vertical columns, assuming that there is no horizontal background error covariance. The rationale behind it is to find vertical profiles of cloud liquid and ice water content that yield the observed cloud optical thickness values and are consistent with the simulated profile. Afterwards, a latent heat adjustment is applied to the temperature in the vertical column. Data from 4 meteorological surface stations around Paris are used to verify the model simulations. The results show that the presented assimilation procedure is able to improve the simulated 2 m air temperatures and incoming shortwave radiation significantly during cloudy days. The scheme is able to alter the position of the cloud fields significantly and brings the simulated cloud pattern closer to the observations. As the scheme is rather simple and computationally fast, it is a promising new technique to improve the surface fields of retrospective model simulations for variables that are affected by the position of the clouds.

1 Introduction

Mesoscale atmospheric models are used extensively to reconstruct high-resolution regional atmospheric conditions as an input for e.g. hydrological, land surface or air pollution models. Although sophisticated techniques are used to parameterize clouds and precipitation, a large source of uncertainty in the model results remains in predicting the location of cloud systems at high spatial resolutions. As clouds have a strong

ACPD
11, 13355–13380, 2011

impact on the surface energy budget and hence the local temperatures, an inaccurate simulation of the overlying cloud cover is problematic for certain applications that need correct surface input data. The assimilation of satellite data into the atmospheric model can play an important role in providing improved model results on a local scale.

Cloud assimilation studies have focused mainly on cloud retrievals from radar data, either with one-dimensional variational schemes (1DVAR) (Benedetti et al., 2003) or with more complex models in 3DVAR (Hu et al., 2006a, b) and 4DVAR (Sun and Crook, 1998; Vukićević et al., 2004). Recently, Benedetti and Janisková (2008) used a 4DVAR system to assimilate Moderate Resolution Imaging Spectroradiometer (MODIS) cloud optical depth observations into the European Centre for Medium range Weather Forecast (ECMWF) model. Their results show a positive impact on certain variables like the distribution of cloud ice water content but the assimilation did not always improve the analysis fit to the observations. However, the complexity of developing and maintaining the adjoint code needed by these techniques and their high computational costs for high-resolution applications are limiting their use in research.

Other simpler and faster methods exist that attempt to retrieve model cloud microphysics from satellite observations or other sources. Soutu et al. (2003) constructed cloud fields for their forecasts over the Galician Region in Spain based on relative humidity values from the NCEP Aviation Model. Their procedure followed the Local Analysis and Prediction System (LAPS, Albers et al., 1996) and clearly improved the model's skill to predict precipitation amounts. Another method is used by Yucel et al. (2003), who applied a nudging assimilation technique to ingest remotely sensed cloud cover and cloud top height data into their mesoscale atmospheric model. The cloud ingestion was found to improve the ability of the model to capture the variation in surface fields associated with cloud cover. However, they suggested that it would be necessary to modify the model dynamics and thermodynamics to be consistent with the ingested cloud fields.

In this context, the goal of the research reported here is to present a rather simple and computational fast cloud assimilation scheme. The scheme applies optimal

ACPD
11, 13355–13380, 2011

interpolation with latent heat adjustment for the assimilation of cloud optical thickness (COT) observations into a mesoscale atmospheric model to study the effect on the simulated surface fields associated with cloud cover. The model used for this study is the Advanced Regional Prediction System (ARPS), a non-hydrostatic mesoscale atmospheric model developed at the University of Oklahoma (Xue et al., 2000, 2001). Although the ARPS model has its own cloud analysis package (ADAS, Brewster, 1996), it is not used in our study because the cloud optical thickness data do not contain any vertical information which is needed by ADAS.

The remainder of the paper is organized as follows. A description of the atmospheric model and a set-up for the model simulations are given in Sect. 2. In Sect. 3, the details of the cloud assimilation scheme are presented. The results are evaluated and discussed in Sect. 4 while conclusion are given in Sect. 5.

2 Numerical model and data description

The Advanced Regional Prediction System (ARPS) includes conservation equations for momentum, heat, mass, water (vapour, liquid and ice), sub-grid scale turbulent kinetic energy and the state-equation of moist air. The finite-difference equations of the model are discretized on an Arakawa C-grid, employing a terrain following coordinate in the vertical direction. Advection is solved with a fourth-order central differencing scheme and leapfrog time stepping. Turbulence is represented by the 1.5-order turbulent kinetic energy (TKE) model, and the Sun and Chang (1986) parameterization for the convective boundary layer. The 6-category water/ice scheme of Lin et al. (1983) accounts for the model microphysics while the Kain-Fritsch cumulus parameterization scheme solves the cumulus convection (Kain and Fritsch, 1990). In order to suppress numerical noise, a fourth-order monotonic computational mixing was applied, following Xue (2000).

Land surface processes are parameterized by the Soil-Vegetation-Atmosphere Transfer model of De Ridder and Schayes (1997). To two primary parameters of the land surface model are the type of vegetation, which is derived from the Coordination

ACPD
11, 13355–13380, 2011

Information Environment (CORINE) land cover data and the soil texture, which is assumed to be that of a loamy soil, homogeneous across the domain. Among the secondary parameters, vegetation fraction is based on the normalized difference vegetation index (NDVI) from the SPOT-VEGETATION satellite imagery.

Data with a 0.25° horizontal resolution from the global operational analysis by the ECMWF are used as initial conditions and as 6-hourly lateral boundary conditions for the model runs. The ARPS model domain has a grid spacing of 16 km and a domain size of 1600 km × 1600 km, centred over Paris (Fig. 1). In all simulations, 35 vertical levels are employed with a grid spacing of 25 m near the surface increasing to 1 km near the upper model boundary, located at 20 km altitude. The simulations are initialized on 1 June 2006 at 00:00 LT and run until 30 June 2006 at 24:00 LT. This month is chosen to test our assimilation scheme as during some periods of this month, the model has problems in simulating the right amount and position of clouds, which leads to large errors in some surface variables as will be shown in Sect. 4.

The cloud optical thickness images for June 2006 are retrieved from visible and shortwave infrared imagery from the Spinning Enhanced Visible and Infrared imager (SEVIRI) onboard the Meteosat Second Generation satellite with a semi-analytical cloud retrieval algorithm (Pandey et al., 2011). This algorithm is based on the retrieval algorithm of Kokhanovsky et al. (2003) for the estimation of cloud optical thickness. The details of the scheme can be found in Pandey et al. (2011). As Meteosat is a geostationary satellite, the algorithm provides COT images every quarter of an hour during daytime (06:00–20:00 LT). These images are assimilated every 15 min into the ARPS model following the procedure that is explained in Sect. 3.

To test the effect of our cloud assimilation procedure, 2 m air temperature and specific humidity data for 2 observational stations close to Paris (Melun and Trappes, Fig. 1) are gathered from the National Climatic Data Center (NCDC) dataset. Furthermore, 2 m air temperature, specific humidity and incoming shortwave radiation data for 2 more stations (Fontainbleau and Grignon, Fig. 1) are taken from the CarboEurope Integrated Project.

ACPD
11, 13355–13380, 2011

3 Cloud optical thickness assimilation procedure

The data assimilation procedure applied in this study calculates 3-D analysis fields of specific cloud liquid and ice water content (q_c and q_i) and operates on 1-D vertical columns. The rationale behind the method is to find vertical profiles of q_c and q_i that yield the observed cloud optical thickness fields τ_0, and that are consistent with the background (simulated) profile, in the sense that clouds are put in layers with a large humidity. This a priori assumption is required as τ_0 does not contain height information.

3.1 Background COT

Consider a vertical model column containing n grid cells irregularly spaced at positions z_i ($i = 1,...,n$), starting from the surface. Each layer (thickness Δz_i) is characterized by a simulated specific cloud water content q_{cbi}, which can be either liquid or solid (ice) water. Noting that the quantity $\rho_i q_{cbi} \Delta z_i$ is the incremental liquid/ice water path (in $\mathrm{kg\,m^{-2}}$) of layer i (ρ_i being the air density of layer i), the incremental optical depth contributed by layer i is given by (Kokhanovsky, 2006):

$$\Delta\tau_{bi} = \frac{3}{2\rho_w}\frac{\rho_i q_{cbi}}{r_{ei}}\Delta z_i \tag{1}$$

with $\rho_w = 1000\,\mathrm{kg\,m^{-3}}$ the density of liquid water, and r_{ei} the effective radius of cloud droplets in layer i, which is parameterized in ARPS as a function of temperature, to account for the different values of this quantity for liquid versus solid water.

The full model-based columnar optical depth is then given by:

$$\tau_b = \sum_{i=1}^{n}\Delta\tau_{bi} = \frac{3}{2\rho_w}\sum_{i=1}^{n}\frac{\rho_i q_{cbi}}{r_{ei}}\Delta z_i = \frac{3}{2\rho_w}\left(\frac{\rho_1\Delta z_1}{r_{e1}}\cdots\frac{\rho_n\Delta z_n}{r_{en}}\right)\begin{pmatrix} q_{cb1} \\ . \\ . \\ . \\ q_{cbn}\end{pmatrix} \equiv \mathbf{H}\boldsymbol{q}_{cb} \tag{2}$$

ACPD
11, 13355–13380, 2011

H is a so-called observation operator, which linearly maps q_{cb} onto a background (i.e., simulated) optical thickness ($\tau_b = \mathbf{H}q_{cb}$).

3.2 Optimal interpolation

Given observations of cloud optical thickness for a given position on the globe, the best linear unbiased estimate of cloud water content is given by (Kalnay, 2003):

$$q_{ca} = q_{cb} + \mathbf{K}(\tau_0 - \mathbf{H}q_{cb}) \tag{3}$$

with q_{ca} the vector containing the analyzed cloud water content values at level i, and q_{cb} likewise containing the values generated by the model ("background" or first guess value). The gain matrix is given by

$$\mathbf{K} = \mathbf{B}\mathbf{H}^T(\mathbf{H}\mathbf{B}\mathbf{H}^T + \mathbf{R})^{-1} \tag{4}$$

with $\mathbf{B}$ the background error covariance matrix and $\mathbf{R}$ ($\equiv\sigma_\tau^2$) the observation error covariance, which in this case is a scalar since τ_0 itself is a scalar quantity.

We will assume that $\mathbf{B}$ is a diagonal matrix. This is not entirely realistic, since errors of cloud water content at different vertical layers may be correlated, especially if these layers are close to each other in comparison to the typical thickness of a cloud layer. Nevertheless, it is difficult to estimate these inter-layer correlations and, moreover, the thicknesses of the layers that are prone to cloud development (sufficiently far away from the surface) are rather thick, thus making this diagonality assumption less of a problem. A diagonal background error covariance matrix has the advantage of leading to a fairly simple final expression for the analyzed specific cloud water content, as shown below.

Indeed, in case $\mathbf{B}$ is a diagonal matrix with elements $\sigma_{ci}^2\delta_{ij}$ (with δ_{ij} the Kronecker delta), one has:

$$\mathbf{H}\mathbf{B}\mathbf{H}^T + \mathbf{R} = \sum_{i=1}^{n} \sigma_{ci}^2 h_i^2 + \sigma_\tau^2$$

$$\mathbf{B}\mathbf{H}^T = (\sigma_{c1}^2 h_1 \ldots \sigma_{cn}^2 h_n)^T \tag{5}$$

ACPD
11, 13355–13380, 2011

with h_i the operation operator for layer i. This leads, finally, to:

$$q_{\mathrm{ca}i} = q_{\mathrm{cb}i} + \frac{\sigma_{\mathrm{c}i}^2 h_i}{\sum_{i=1}^{n} \sigma_{\mathrm{c}i}^2 h_i^2 + \sigma_\tau^2} \left(\tau_0 - \sum_{i=1}^{n} h_i q_{\mathrm{cb}i} \right) \tag{6}$$

The main challenge is to specify the $\sigma_{\mathrm{c}i}$ in a suitable manner, in particular in such a way that model layers with a high simulated humidity are more affected than the drier layers.

3.3 Cloud water background error variance

The specification of the cloud water background error variance $\sigma_{\mathrm{c}i}$ of each model layer is not straightforward, in particular when a layer contains no simulated liquid or ice water ($q_{\mathrm{cb}i} = 0$). One might be tempted to set $\sigma_{\mathrm{c}i} = 0$ in such a situation, but from the analysis equation above it is clear that $q_{\mathrm{zca}i}$ will also be zero then, even if a cloud is observed ($\tau_0 > 0$). Clearly, a non-zero cloud water background error variance must be assigned, even for non-saturated layers. Simply taking $\sigma_{\mathrm{c}i}$ as a fraction of $q_{\mathrm{cb}i}$ will not work for the reasons just explained. The background error variance matrix will therefore be established starting from a probability density function for total specific water content q_{t}, which is defined as the sum of vapour and cloud (liquid/ice) contributions, i.e., $q_{\mathrm{t}} = q_{\mathrm{v}} + q_{\mathrm{c}}$. The goal is now to find the cloud water content error, given the error on total water content. The error on the latter needs to be specified a priori, in our case this will be done as a fixed fraction of total water content (see Sect. 3.4).

We employ a normal distribution, given by:

$$f(q_{\mathrm{t}}) = \frac{1}{\sqrt{2\pi}\sigma_{\mathrm{t}}} e^{-\frac{(q_{\mathrm{t}} - q_{\mathrm{t}b})^2}{2\sigma_t^2}} \tag{7}$$

with q_{tb} the background (simulated) value of q_{t}, and σ_{t} the standard deviation of the distribution, which is a measure for the error on simulated total water q_{t}. Figure 2 presents the concept of the normal distribution of q_{t}.

ACPD
11, 13355–13380, 2011

Cloud water is that portion of q_t which is in excess of the saturated value, denoted q_s ($\equiv q_{sat}(T)$), with T the temperature of the considered layer, so that $q_c = (q_t - q_s)H(q_t - q_s)$, with $H(.)$ the Heaviside step function, which is unity for a positive argument and zero otherwise. Using this, taking the simulated cloud water content q_{cb} as expected value for this quantity, and omitting the layer index i for the moment, the error variance of simulated cloud water can be calculated as follows:

$$\sigma_c^2 = \int_{-\infty}^{+\infty} (q_c - q_{cb})^2 f(q_t) dq_t = \int_{q_s}^{+\infty} [(q_c + q_s) - (q_{cb} + q_s)]^2 f(q_t) dq_t = \int_{q_s}^{+\infty} (q_t - q_{tb})^2 f(q_t) dq_t \quad (8)$$

such that:

$$\sigma_c^2 = \frac{1}{\sqrt{2\pi}\sigma_t} \int_{q_s}^{+\infty} (q_t - q_{tb})^2 e^{\frac{q_t - (q_{tb})^2}{2\sigma_t^2}} dq_t$$

$$= \frac{2\sigma_t^2}{\sqrt{\pi}} \int_{x_s}^{+\infty} x^2 e^{-x^2} dx \sigma_c^2 = \sigma_t^2 \left[\frac{1}{2} \mathrm{erfc}(x_s) + \frac{x_s}{\sqrt{\pi}} e^{-x_s^2} \right] \quad (9)$$

with $x_s = \frac{q_s - q_{tb}}{\sqrt{2}\sigma_t}$ and erfc(.) the complementary error function.

3.4 Implementation in the ARPS model

In the above, the standard deviation on the simulated total water content and the observed cloud optical thickness are still unknown. These standard deviations are expressed as a fraction of q_t and τ_0, respectively, i.e. $\sigma_t = aq_t$ and $\sigma_\tau = b\tau_0$. In our study, a value of 0.3 is adopted for coefficient a (i.e., ±30% error of q_t). Based on a validation study of our cloud optical thickness product with Cloudsat COT data (Pandey et al., 2011), a rather conservative value of 0.25 is adopted for coefficient b (i.e. ±25% error of τ_0), with a lower limit of 5 for σ_τ.

ACPD
11, 13355–13380, 2011

The resulting q_{ca} from the assimilation procedure is defined as cloud liquid water when the temperature is warmer than −10 °C, and as cloud ice when the temperature is colder than −30 °C. A linear ramp is applied for the temperature in between. Whenever a non-saturated (and cloudless) layer becomes cloudy after the analysis, the specific humidity is set to its saturated value. Last, a latent heat adjustment to temperature based on the added or subtracted amounts of q_c and q_i is applied, according to the formula:

$$\Delta T_{q_c} = \Delta q_c \frac{L_v}{C_p} \tag{10}$$

$$\Delta T_{q_i} = \Delta q_i \frac{L_v + L_f}{C_p} \tag{11}$$

where L_v and L_f are the latent heat of vaporization and fusion at 0 °C respectively, and C_p is the specific heat of dry air at constant pressure.

4 Results of the assimilation procedure

This section describes the results for a COT assimilation experiment (EXP) for the month of June 2006, compared to a reference simulation (REF) with a setup identical to the cloud assimilation experiment to provide a benchmark for the effect of the introduction of cloud optical thickness data.

4.1 Comparison to observations

Figure 3 shows the impact of the COT assimilation on 2 m air temperatures, measured at 2 stations close to Paris. It is apparent that the reference simulation does not correctly capture a sharp temperature decrease halfway the month (14 and 15 June) and keeps on overestimating the temperatures around noon by a few degrees during the rest of the month. This is substantially improved by the COT assimilation which picks

ACPD
11, 13355–13380, 2011

up the temperature decrease on 15 June and the following days. The problems for the reference simulation are caused by a wrong location of a cold front and associated overlying cloud cover during these days, as will be shown later on. The assimilation procedure is thus capable of improving the cloud fields and yielding more accurate temperature values. Note that sometimes also the temperature during night time improves in the EXP simulation (e.g. on 28 June in Melun) although the assimilation scheme is only active during day time. This is due to the transportation of the assimilated moisture throughout the model domain.

These findings are further demonstrated in Table 1, which shows the results for all 4 observation stations around Paris. The COT assimilation decreases the positive bias that is present in the reference simulation and reduces the root-mean-square error (RMSE) between modelled and observed values. Also the correlation coefficients between the modelled and observed time series are higher for the assimilation experiment.

Another variable that is closely linked to the cloud fields, is the surface shortwave radiation. The results for the observation stations of Grignon and Fontainbleau are presented in Fig. 4 and Table 2. As for the temperature, the COT assimilation experiment clearly improves the time series, especially on the problematic days of 14 and 15 June. The statistics show a substantial reduction of the bias and RMSE and higher correlation coefficients. These numbers confirm that the improvement in the assimilation experiment is linked to a better position of the cloud cover in the model.

However, the impact of the COT assimilation is not positive for all variables, as shown in Table 3. The specific humidity at the surface is in good agreement with the observations for the reference simulation, whereas it is overestimated by about 1 $g\,kg^{-1}$ when the assimilation scheme is applied. The extra moisture is caused by the fact that the assimilation scheme sets the humidity of a layer to its saturated value whenever a non-saturated layer becomes cloudy. As the reference simulation underestimates the amount of clouds compared to the observations, an increase of the humidity is the logical consequence in this case. This can not be avoided if we want to retain the

ACPD
11, 13355–13380, 2011

assimilated clouds, otherwise they would evaporate instantly. In their cloud assimilation experiments, Benedetti and Janiskova (2008) also noticed that the humidity was affected in a slightly negative way by the assimilation.

4.2 Impact on temperature, humidity and cloud parameters

To assess the impact of the assimilation procedure on the model variables in the entire model domain, mean zonal differences between the experiment and the reference for temperature and specific humidity are shown in Fig. 5. The assimilation clearly has the largest effect in the lowest 2000 m of the model domain. Here, the temperature values of the experiment have a tendency to be lower (up to 0.5 K) while the specific humidity is augmented (up to 0.5 g kg^{-1}). Both temperature and moisture changes are in phase to enhance cloud formation. In the upper levels, a slight temperature increase is visible for the assimilation experiment, which is caused by latent heat release during the formation of additional clouds. As shown in the previous section, the temperature decrease near the surface improves the positive bias in the reference simulation, while the moisture increase has a negative effect when compared to the observations.

As a response to the changes in temperature and humidity in the assimilation experiment, there is a noticeable redistribution in liquid water path and ice water path in the model domain (Fig. 6). The changes appear to have a rather varied structure over the largest part of the model domain. Most positive changes occur along the southern boundary of the domain and over the alpine region. Overall, there is a clear tendency of increased cloud amounts in the assimilation experiment. The monthly mean values of the liquid and ice water paths are raised by 25 and 8 % respectively. Regarding the overestimation of incoming shortwave radiation by the reference simulation (Table 2), these changes appear to have a positive impact on the model results.

Finally, the direct impact of the COT assimilation on the modelled cloud fields is presented in Fig. 7. In this figure the position of the clouds is shown on 15 July at noon, when a cold front passes Paris which is not picked up in the reference simulation (Fig. 3). The clouds are positioned too far to the east and there is no strong front

ACPD
11, 13355–13380, 2011

structure visible. The COT assimilation scheme is able to alter the cloud structure significantly and brings it much closer to the observations over the central region of the model domain. Although the scheme is not able to get rid entirely of the overestimation of clouds in the west side of the model domain, it is clearly able to improve the model simulation.

5 Discussion and conclusions

In this paper, a technique has been presented to assimilate cloud optical thickness information into a mesoscale atmospheric model to yield improved diagnoses of surface solar radiation and temperature. The technique comprises an optimal interpolation of cloud liquid and ice water in 1-D vertical columns together with a latent heat adjustment. The scheme requires some assumptions including the absence of horizontal background error covariance, but it is rather simple and computationally fast, especially when compared to the 4DVAR systems that are currently developed (e.g. Benedetti and Janisková, 2008). The goal of the assimilation scheme is to improve retrospective model simulations by feeding the model with observed cloud optical thickness images every 15 min.

Results for the month of June 2006 over Paris show a positive impact of the assimilation on near-surface temperatures and incoming shortwave radiation, two variables that are closely linked to the overlying cloud cover and are crucial as input in, for instance, air pollution models. However, comparison to specific humidity observations show that the changes induced by the assimilation do not always improve the model fit to the observations. The assimilation scheme tends to induce overestimations of humidity due to the fact that a layer is set to saturation when it becomes cloudy. This is necessary to retain the new clouds in the model and the same technique is used in the cloud analysis scheme of Soutu et al. (2003). Although the moisture field in the lowest 2000 m of the model domain is affected in a slightly negative way, the results show that the position of the cloud fields are more accurately simulated when the cloud observations are assimilated.

ACPD
11, 13355–13380, 2011

We can thus conclude that it is feasible to introduce the presented COT assimilation procedure in a mesoscale atmospheric model without disrupting the model stability. As the procedure is simple and fast, it is a promising new technique to improve the quality of surface level model output of retrospective simulations.

Acknowledgements. This research has been performed in the framework of the Climate and Air Quality Modelling for Policy Support (Climaqs) project, sponsored by the Flemish agency for Innovation by Science and Technology, and the FP-7 Myair PASODOBLE project, sponsored by the European Commission's Seventh Framework Programme. We would like to thank the following CARBOEUROPE PIs for providing access to their data: Jean-Yves Pontailler (FR-FON) and Nicolas Mascher (FR-GRI). We also acknowledge the National Climatic Data Center (NCDC) for providing valuable validation data. The ARPS meteorological model was made available by the Center for Analysis and Prediction of Storms at the University of Oklahoma. We would also like to acknowledge the European Environment Agency for making available the CORINE land-cover data, the U.S. Geological Survey for the GTOPO30 dataset, the Jet Propulsion Laboratory for the SST imagery, NASA's Earth Science Division for the GLDAS data, and our VITO colleagues at TAP for the SPOT-VEGETATION NDVI imagery. Meteorological forcing data were obtained from the European Centre for Medium-Range Weather Forecasting (ECMWF).

References

Albers, S. C., McGinley, J. A., Birkenheuer, D. A., and Smart, J. R.: The Local Analysis and Prediction System (LAPS): Analysis of clouds, precipitation and temperature, Weather Forecast., 11, 273–287, 1996.

Benedetti, A. and Janisková, M.: Assimilation of MODIS Cloud Optical Depths in the ECMWF Model, Atmos. Rev., 136, 1727–1747, 2008.

Benedetti, A., Stephens, G. L., and Vukićević, T.: Variational assimilation of radar reflectivities in a cirrus model. I: Model description and adjoint sensitivity studies, Q. J. Roy. Meteor. Soc., 129, 277–300, 2003.

Brewster, K.: Application of a Bratseth analysis scheme including Doppler radar data. Preprints, 15th Conf. Wea. Anal. Forecast. Amer. Meteor. Soc., Norfolk, VA, 92–95, 1996.

ACPD

11, 13355–13380, 2011

DeRidder, K. and Schayes, G.: The IAGL land surface model, J. Appl. Meteorol., 36, 167–182, 1997.
Hu, M., Xue, M., and Brewster, K.: 3D-VAR and cloud analysis with WSR-88D level-II data for the prediction of the Fort Worth, Texas, tornadic thunderstorms. Part I: Cloud analysis and its impact, Mon. Weather Rev., 134, 675–698, 2006a.
Hu, M., Xue, M., and Brewster, K.: 3D-VAR and cloud analysis with WSR-88D level-II data for the prediction of the, Fort Worth, Texas, tornadic thunderstorms. Part II: Impact of radial velocity analysis via 3D-VAR, Mon. Weather Rev., 134, 699–721, 2006b.
Kain, J. S. and Fritsch, J. M.: A One-Dimensional Entraining Detraining Plume Model and Its Application in Convective Parameterization, J. Atmos. Sci., 47, 2784–2802, 1990.
Kalnay, E.: Atmospheric modeling, data assimilation and predictability, Cambridge Univ. Press, 341 pp., 2003.
Kokhanovsky, A. A., Rozanov, V. V., Zege, E. P., Bovensmann, H., and Burrows, J. P.: A semi-analytical cloud retrieval algorithm using backscattered radiation in 0.4–2.4μm spectral region, J. Geophys. Res., 108, 4008, doi:10.1029/2001JD001543, 2003.
Kokhanovsky, A. A.: Cloud Optics, Berlin: Springer-Verlag, 2006.
Lin, Y.-L., Farley, R. D., and Orville, H. D.: Bulk parameterization of the snow field in a cloud model, J Clim. Appl. Meteor., 22, 1065–1092, 1983.
Pandey, P., De Ridder, K., and van Lipzig, N. P. M.: Estimating scaled cloud optical thickness from SEVIRI by implementing a semi-analytical cloud retrieval algorithm, Atmos. Res., in review, 2011.
Soutu, M. J., Balseiro, C. F., Pérez-Munuzuri, V., Xue, M., and Brewster, K.: Impact of Cloud Analysis on Numerical Weather Prediction in the Galician Region of Spain, J. Appl. Meteorol., 42, 129–140, 2003.
Sun, W. Y. and Chang, C. Z.: Diffusion-Model for a Convective Layer .1. Numerical-Simulation of Convective Boundary-Layer, J. Clim. Appl. Meteorol., 25, 1445–1453, 1986.
Sun, J. and Crook, N. J.: Dynamical and microphysical retrieval from Doppler radar observations using a cloud model and its adjoint. Part II: Retrieval experiments of an observed Florida convective storm, J. Atmos. Sci., 55, 835–852, 1998.
Vukićević , T., Greenwald, T., Županski, M., Županski, D., Vonder Haar, T., and Jones, A. S.: Mesoscale cloud state estimation from visible and infrared satellite radiances, Mon. Weather Rev., 132, 3066–3077, 2004.
Xue, M.: High-order monotonic numerical diffusion and smoothing, Mon. Weather Rev., 128,

ACPD
11, 13355–13380, 2011

2853–2864, 2000.
Xue, M., Droegemeier, K. K., and Wong, V.: The Advanced Regional Prediction System (ARPS) – A multi-scale nonhydrostatic atmospheric simulation and prediction model. Part I: Model dynamics and verification, Meteorol. Atmos. Phys., 75, 161–193, 2000.
Xue, M., Droegemeier, K. K., Wong, V., Shapiro, A., Brewster, K., Carr, F., Weber, D., Liu, Y., and Wang, D.: The Advanced Regional Prediction System (ARPS) – A multi-scale nonhydrostatic atmospheric simulation and prediction tool. part II: Model physics and applications, Meteorol. Atmos. Phys., 76, 143–165, 2001.
Yucel, I., Shuttleworth, W. J., Gao, X., and Sorooshian, S.: Short-term Performance of MM5 with Cloud-Cover Assimilation from Satellite Observations, Mon. Weather Rev., 131, 1797–1810, 2003.

ACPD
11, 13355–13380, 2011

Table 1. Statistics of the 2 m air temperature for the entire month of June 2006.

T (K)	Mean	Bias	RMSE	R^2
Melun				
Obs	291.22	–	–	–
REF	291.75	0.53	2.64	0.85
EXP	291.17	−0.05	1.94	0.89
Grignon				
Obs	290.34	–	–	–
REF	291.68	1.34	2.95	0.84
EXP	291.00	0.66	2.14	0.87
Trappes				
Obs	291.43	–	–	–
REF	291.73	0.30	3.11	0.79
EXP	291.06	−0.37	2.51	0.82
Fontainbleau				
Obs	290.83	–	–	–
REF	291.92	1.09	3.58	0.76
EXP	291.35	0.52	2.83	0.80

ACPD
11, 13355–13380, 2011

Table 2. Statistics of the incoming shortwave radiation for the entire month of June 2006.

R_s (W m^{-2})	Mean	Bias	RMSE	R^2
Grignon				
Obs	360.30	–	–	–
REF	416.12	55.82	156.35	0.77
EXP	400.72	40.42	124.02	0.84
Fontainbleau				
Obs	381.90	–	–	–
REF	430.69	48.79	157.24	0.77
EXP	410.46	28.56	119.35	0.85

ACPD
11, 13355–13380, 2011

Table 3. Statistics of the 2 m specific humidity for the entire month of June 2006.

q (g kg^{-1})	Mean	Bias	RMSE	R^2
Melun				
Obs	8.67	–	–	–
REF	8.70	0.03	1.35	0.56
EXP	9.62	0.95	1.89	0.50
Grignon				
Obs	8.67	–	–	–
REF	8.64	−0.03	1.26	0.58
EXP	9.44	0.77	1.66	0.54
Trappes				
Obs	8.45	–	–	–
REF	8.60	0.15	1.36	0.54
EXP	9.46	1.01	1.91	0.48
Fontainbleau				
Obs	8.60	–	–	–
REF	8.67	0.07	1.37	0.57
EXP	9.60	1.00	1.92	0.51

ACPD
11, 13355–13380, 2011

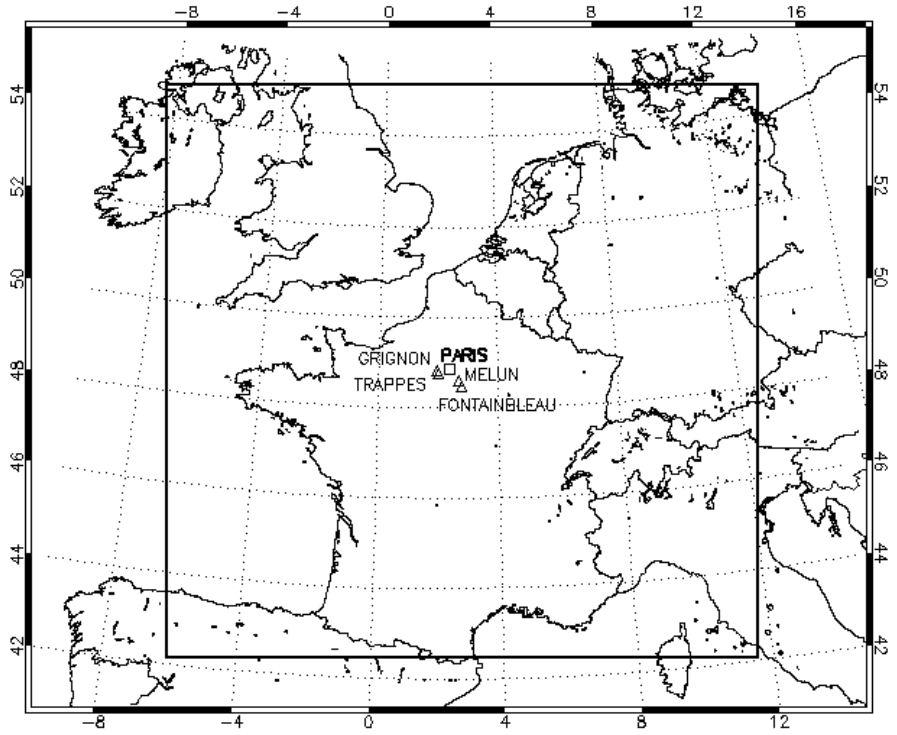

Fig. 1. Location of the model domain and the observational stations.

ACPD
11, 13355–13380, 2011

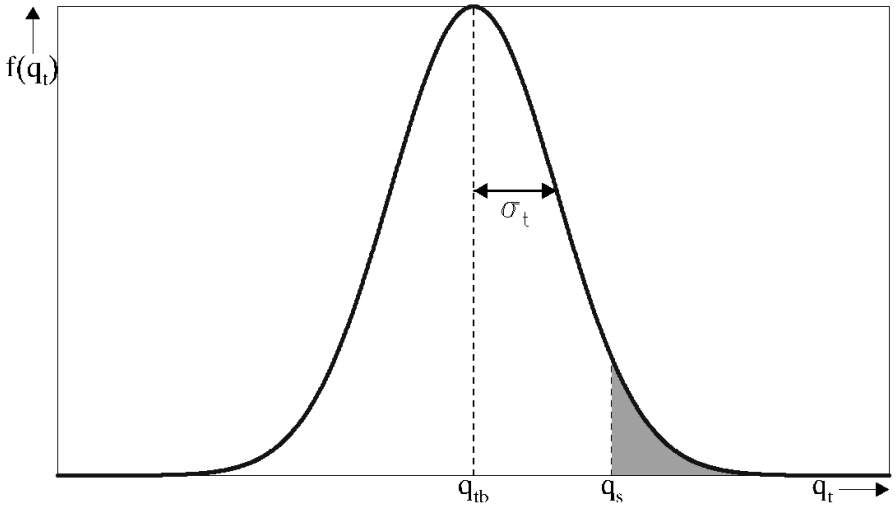

Fig. 2. Probability distribution function for total water content (blue line), with expectation value q_{tb}, and standard deviation σ_t. The light shading corresponds to the area above the saturated specific humidity (denoted q_s), which contains cloud water.

ACPD
11, 13355–13380, 2011

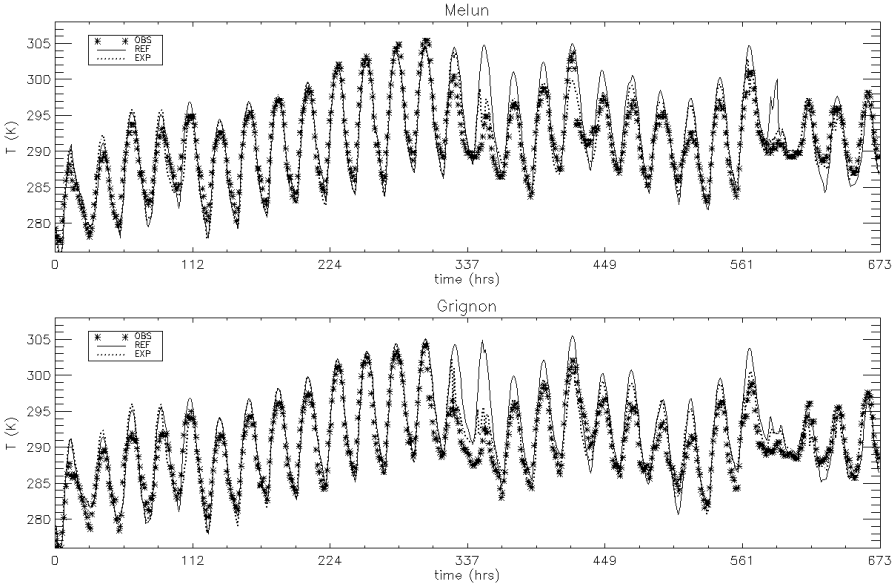

Fig. 3. 2 m air temperature at Melun (upper panel) and Grignon (lower panel) for June 2006.

ACPD
11, 13355–13380, 2011

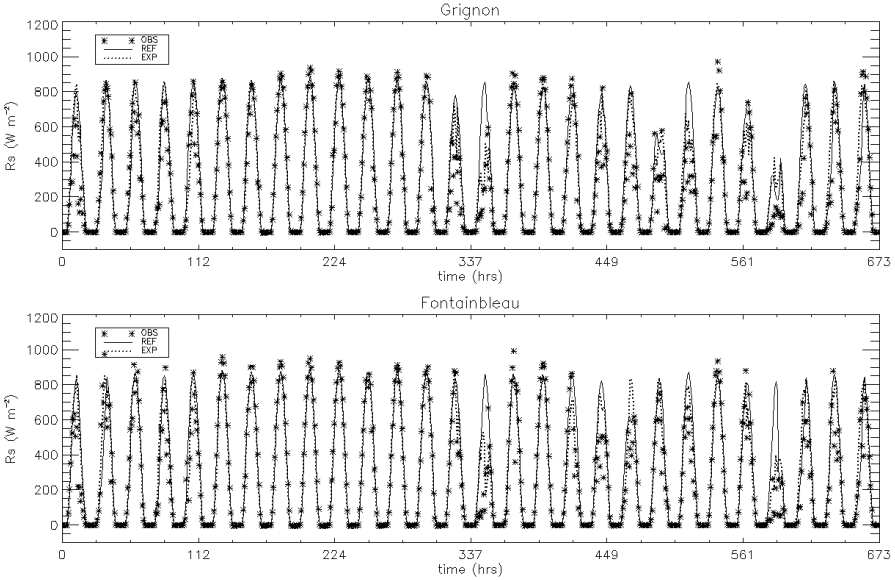

Fig. 4. Incoming shortwave radiation at Grignon (upper panel) and Fontainbleau (lower panel) for June 2006.

ACPD
11, 13355–13380, 2011

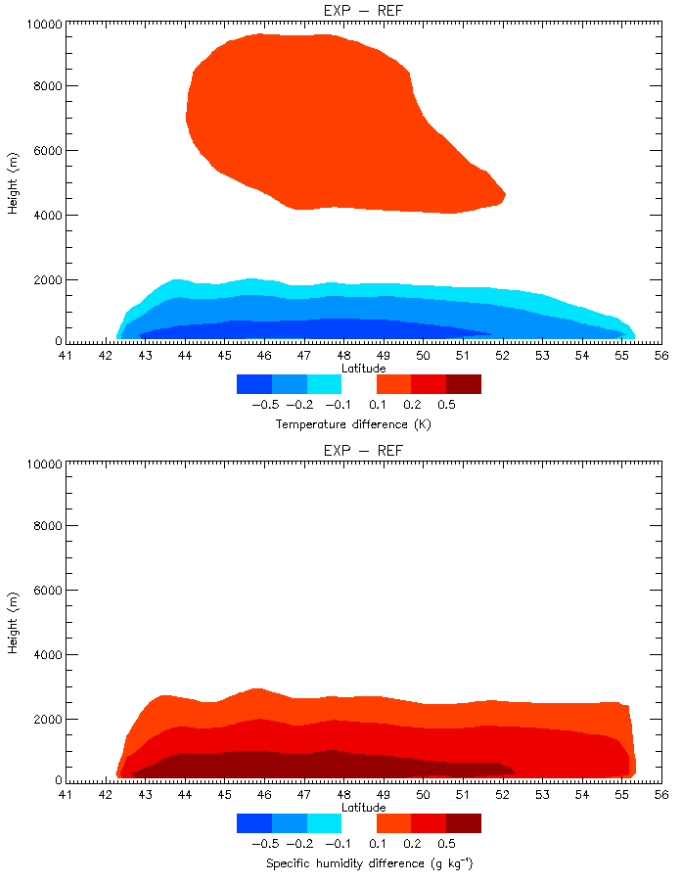

Fig. 5. Upper panel: temperature difference between the COT assimilation experiment and the Reference simulation for the entire month of June 2006 and averaged per latitude band. Lower panel: specific humidity difference between the COT assimilation experiment and the Reference simulation for the entire month of June 2006 and averaged per latitude band.

ACPD
11, 13355–13380, 2011

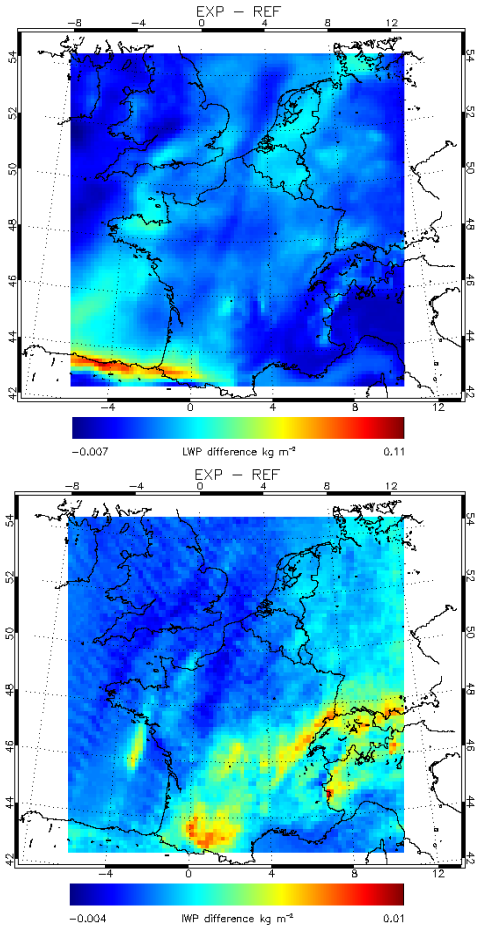

Fig. 6. Monthly mean difference in liquid water path (upper panel) and ice water path (lower panel) between the COT assimilation experiment and the Reference simulation.

ACPD
11, 13355–13380, 2011

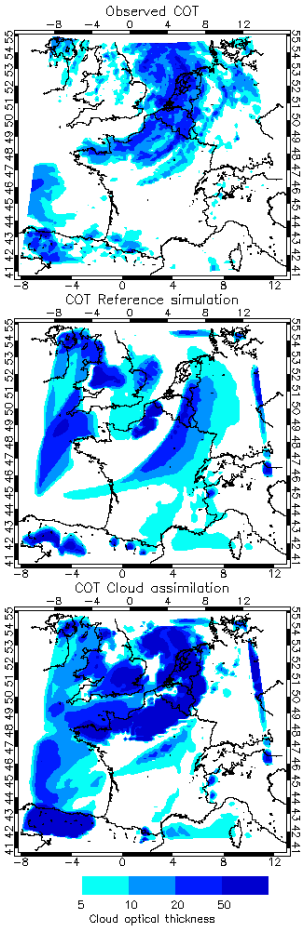

Fig. 7. Cloud optical thickness maps on 15 June 2006 at 12:00 LT.

ACPD
11, 13355–13380, 2011